Sedimentary Geology 429 (2022) 106081

Contents lists available at ScienceDirect

Sedimentary Geology

journal homepage: www.elsevier.com/locate/sedgeo

Spatial self-organization of marine agglutinated microbial carbonate build-ups: Insights from stratigraphic forward modelling using Stromatobyte3D

Haiwei Xi [a,*], Peter M. Burgess [a], Estanislao Kozlowski [b], David W. Hunt [c], Alexandra Jurkiw [c], Isabella Masiero [c]

[a] Quantitative Experimental Stratigraphy Group, Jane Herdman Laboratory, Department of Earth, Ocean and Ecological Science, University of Liverpool, Brownlow Street, Liverpool L69 3GP, UK
[b] Department of Earth Sciences, Royal Holloway, University of London, Egham TW20 0EX, UK
[c] Equinor ASA, Norway, Sandsliveien 90, Sandsli, Bergen, Norway

ARTICLE INFO

Article history:
Received 14 November 2021
Received in revised form 6 January 2022
Accepted 7 January 2022
Available online 14 January 2022

Editor: Dr. Brian Jones

Keywords:
Microbialite
Self-organization
Autogenic
Stratigraphic forward model
Sedimentary record

ABSTRACT

Microbialites span a substantial fraction of Earth history, and have important meanings for understanding long-term history of life and environment. Key controls on microbialite morphology and distribution include substrate topography, hydrodynamic conditions, water depth, salinity, light intensity, and sedimentation rates. This leads to potentially complex combinations of control by internal spatial feedbacks and also external factors. This complexity is explored here using Stromatobyte3D, a new numerical stratigraphic forward model that calculates microbialite accumulation due to in-situ precipitation, sediment trapping and binding, and sedimentation from suspension, controlled by evolving topography and water flow due to waves, tides or other currents. Results show that with increasingly strong spatial interactions of microbialite growth with water and suspended sediment, particularly the influence of hydrodynamics on in-situ microbialite growth and suspended sediment deposition patterns, three distinct microbialite morphologies are produced, from isolated columns, through elongated mounds, to ridges elongated in the dominant flow direction. Quantitative analysis demonstrates a dominant antecedent substrate topographic control on microbialite nucleation and growth in the absence of water flow, declining as hydrodynamic processes and strong spatial interactions are introduced causing mounds to accrete and coalesce laterally in the flow direction. Formation of coherent morphological patterns, produced by spatial interactions between topography, hydrodynamics, microbialite growth, and sedimentation from suspension, and independent of initial condition, is evidence of spatial self-organization. Modelled morphologies are strikingly similar to observations from modern marine agglutinated microbialite strata, suggesting modelled processes and their behaviours are realistic, and can therefore be useful to assist field interpretations of observed microbialite morphologies where similar processes were operating together.

1. Introduction

Microbialites are organosedimentary deposits produced by benthic microbial communities (Burne and Moore, 1987). Carbonate precipitation is currently considered as the main mechanism for microbialite development, but trapping and binding of allochthonous sediments is also important in modern wave and current-swept marine environments (Monty, 1976; Riding, 2000; Dupraz et al., 2009; Reitner, 2011; Della Porta, 2015; Suarez-Gonzalez et al., 2019). Apart from the various questions about how different biotic and abiotic are involved to form these deposits, a key question is what controls their spatial distribution, and how does this spatial distribution get recorded as heterogenous carbonate strata? Substrate and antecedent karst topography are important controls for coral reef growth and spatial distribution (Purdy and Bertram, 1993), and expected for microbial reefs as well (Grotzinger and Knoll, 1999). For example, microbial colonization and growth appear to have some genetic link to low-relief tepee structures formed during lake level lowstands (Warren, 1982; Coshell et al., 1998; Bouton et al., 2016). These large-scale polygons are well developed in modern marine and non-marine settings, where their density and spacing are laterally variable. If microbialites occurrence and morphology is predominantly dependent on underlying topography (Logan et al., 1974; Ginsburg and Planavsky, 2008), microbialite mound spacing will be similarly variable, difficult to predict and perhaps difficult to interpret in terms of paleoenvironment. However, study from modern coral reef suggests another self-organization possibility (Schlager and Purkis, 2013, 2015; Purkis et al., 2016) that can potentially be applicable to microbial system where spatial interactions between water, topography, sediment transport, and microbialite growth can explain the observed microbialite spatial distributions, such that microbialite mounds self-organize to generate predictable autogenic patterns,

Abbreviations: SSO, Spatial self-organization.

* Corresponding author.
E-mail address: Haiwei.Xi@liverpool.ac.uk (H. Xi).

https://doi.org/10.1016/j.sedgeo.2022.106081
0037-0738/

independent of the initial conditions, and representing an important record of paleoenvironmental conditions.

Previous studies of microbialite morphology and distribution are mostly based on field observations and interpretations, including both modern (Gebelein, 1969; Andres and Reid, 2006; Jahnert and Collins, 2012; Suosaari et al., 2016; Baskin et al., 2021) and ancient examples (Wood et al., 2002; Bosak et al., 2013; Andrews and Trewin, 2014; Bahniuk et al., 2015). However, these studies rarely address how microbial mats interact with adjacent sediment, how the interplay between mound expansion and smothering is linked to macroscopic morphologies, or their large-scale structure and spatial distribution. Also, little emphasis has been placed on experimental and quantitative studies of microbialite growth, to explore how they respond to changes in various environmental factors such as water depth, light intensity, sedimentation rate, and hydrodynamic condition. For example, how microbial mat growth is controlled by substrate topography and how it interacts with sediment flux? What morphology they produce in strata, and how this is reflected on the growth history? Conversely, what factors smother and bury microbial communities, and require recolonisation to recommence deposition? What does this tell us about microbial communities and depositional environment? Characterising, quantifying, and understanding these fundamental processes and their environmental sensitivities with Stromatobyte3D would be an important step forward to fill this gap by testing current hypothesized controlling factors and empirical growth rules.

A recent study of modern microbially-induced bedforms on intertidal flats, shows internal horizontal laminations and regularly spaced ridge-runnel morphological patterns due to extensive biofilm-induced sediment trapping and binding. The patterns are strikingly similar to microbialite strata found in the geological record from the Precambrian onwards (van de Vijsel et al., 2019). Coral reefs grow as individual patches can coalesce and develop reticular patterns in Holocene lagoons due to biotic self-organization (Schlager and Purkis, 2015; Purkis et al., 2016), and in fact microbialites can also develop comparable patterns at scales of tens to hundreds of meters (Dill et al., 1986; Suosaari et al., 2016). Previous numerical modelling (Johnson and Grotzinger, 2006) noted that stromatolites can adjust their column widths during deposition and the effects of initial topography may therefore become progressively weaker as they grow. These studies all display at least one diagnostic feature of spatial self-organization, such as formation of coherent spatial pattern and preferred orientation. Observed features are independent of an initial condition (Levin and Segel, 1985; Purkis et al., 2016), and autogenic in origin, so formed independent of any external forcing (Xi and Burgess, 2022 in press).

To address these questions, a new three-dimensional numerical stratigraphic forward model, Stromatobyte3D, has been developed and integrated with field observation to calculate microbialite accumulation, unravel their complex morphology and spatial distribution in response to external controls, and explore the possibility of self-organizing behaviours as a form of autogenic dynamics in carbonate geomorphic and stratigraphic development.

2. Model formulation and input parameters

Microbialite strata accumulate due to a combination of microbially-induced in-situ precipitation, and trapping and binding of ambient suspended sediment on sticky microbial mats, both controlled by various different biological, chemical and physical processes. Consequently, numerical models of microbialite accumulations require explicit and implicit calculation of several interacting physical, chemical and biological processes. The modelled process and product represent modern agglutinated microbialites in marine environments, such as Shark Bay and the Bahamas, where both in-situ precipitation and sediment trapping and binding are important accumulation processes (Logan, 1961; Dravis, 1983; Reid et al., 2000; Riding, 2011a; Suarez-Gonzalez et al., 2019).

Stromatobyte3D is a reduced-complexity model designed to simulate microbial mound development on the scale of a few meters for each mound. It was modified and developed from a previous model, Mounds3D in Kozlowski (2016). Stromatobyte3D calculates both vertical and lateral microbialite growth, controlled predominantly by hydrodynamic conditions and a background sedimentation rate that deposits non-microbialite lithologies such as packstone and wackestone.

2.1. Calculation of hydrodynamic flow magnitude

Stromatobyte3D includes a simple hydrodynamic model which calculates flow magnitude for each point on the model grid (Fig. 1). This flow magnitude represents flow due to waves and other currents, flowing on one dominant direction (Fig. 1A) but all interacting with the topography they flow over, and time-averaged over the duration of the model time step, in this case one year. A hydrodynamic flow field is calculated that represents a water flux vector in each grid cell, based on flow streamlines that follow the defined dominant direction, but refracted by topography in shallow water (Martinez and Harbaugh, 1989; Burgess and Wright, 2003) (Fig. 1B). Flow magnitude M_{fm}, defined and calculated as the water flux going through each cell, is higher where streamlines converge due to refraction (Fig. 1C), representing a situation where over the course of the whole time step duration, more water flows at relatively higher velocity through the model cell relative to other cells where flow magnitude is lower. A boundary flow magnitude is added to the calculated flow magnitude map, which forces a minimum flow magnitude of 20 streamlines per time step across the whole model grid to ensure some transport of sediment in suspension occurs during each time step.

2.2. Calculation of packstone deposition from suspension

The model can accumulate one of two different lithofacies in any model cell at each time step. A packstone or wackestone lithofacies is deposited due to settling of suspended sediment. Rate of deposition from suspension d_{susp} is controlled by both the topographic gradient and water-flow magnitude. Allochthonous sediment in suspension enters one side of the model grid at a constant rate (Curtis et al., 2021), and deposits packstone at highest rates on grid cells with low surface gradient and low flow magnitude (Fig. 2). Maximum rate of deposition from suspension occurs when surface gradient is zero, and flow magnitude is at the minimum boundary condition value. Conversely, packstone deposition is zero where surface gradient reaches and exceeds the critical angle of repose, or flow magnitude is relatively high and favours grain trapping and binding. The critical angle of repose is set to be 20°, which is a reasonable value for granular silt-sized sediment (Beakawi Al-Hashemi and Baghabra Al-Amoudi, 2018).

2.3. Calculation of microbialite accumulation

At each time-step Δt iteration of the model, the height of each grid cell is updated to reflect accumulation of microbialite structure or deposition of suspended sediment. In Stromatobyte3D, microbial colonization and microbialite accumulation can occur in any grid cell where there is no suspended sediment has been deposited for the last two time step iterations. The effects of microbial colonization R, in-situ precipitation g_p, implicit trapping and binding growth rate g_{tb1} modified by water flow magnitude M_{fm}, a growth term g_d dependent on the bathymetric slope, and explicit trapping and binding growth rate g_{tb2} are all combined to calculate change in height of the topographic cell $\Delta h_{(x,y)}$ such that:

$$\Delta h_{(x,y)} = R_{(x,y)} * \left[\left(g_p + g_{tb2} \right) * \Delta t + \left(g_{tb1} * \Delta t + g_{d(x,y)} \right) * M_{fm(x,y)} \right] \quad (1)$$

where each term is calculated as described in the following sections.

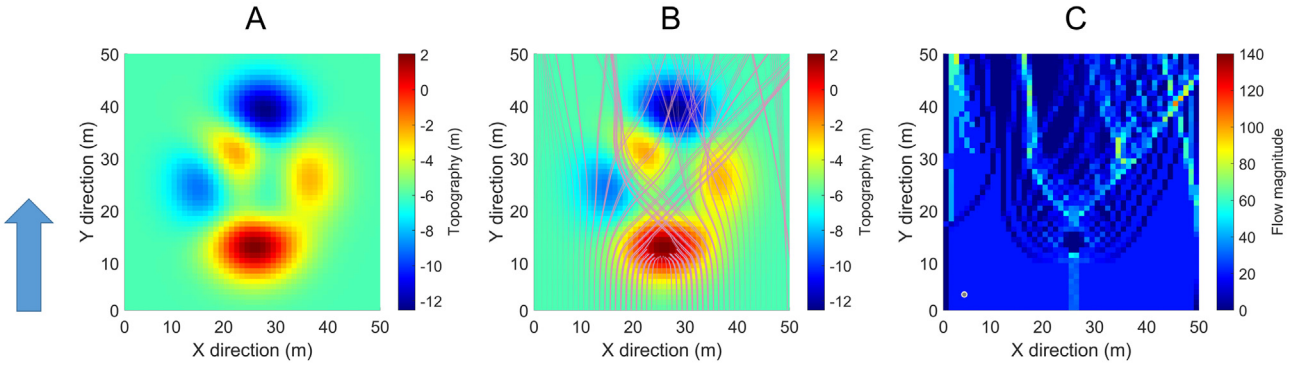

Fig. 1. Details of the hydrodynamic model in Stromatobyte3D. (A) A synthetic topography with an input dominant flow direction from bottom towards the top. (B) Simulated hydrodynamic flow field with multiple flow streamlines on this synthetic topography. Note how they are influenced by topography; some flow lines bend inwards due to refraction when passing the edges of a subaerial barrier (red) and others terminate against the center of this subaerial barrier. Also note flow streamlines diverge and become sparse passing through or by relatively deep areas. (C) Calculated flow magnitude map, showing how higher flow magnitude results from concentrated flow lines, and low flow magnitude results when flow lines diverge. (For interpretation of the references to colour in this figure legend, the reader is referred to the web version of this article.)

2.3.1. Microbialite growth by in-situ precipitation and implicit trapping and binding

Since Stromatobyte3D is designed to model small-scale mound development, it is assumed that maximum in-situ precipitation rate is constant across the model grid and not directly water-depth-dependent. The simplest element of microbialite precipitation is therefore modelled as a spatially-uniform process, controlled by the precipitation rate parameter g_p.

Trapping and incorporation of loose sediment into the microbialites is a complex process, since it depends on the characteristics of the microbial mat, hydrodynamics, and transported sediment in suspension. Water flow is a key environmental factor controlling growth of microbialites due to abundant trapping of sediment, because frequent water movement can mobilize sediments and supply them onto the microbialite surface (Riding, 2000; Andres and Reid, 2006; Suarez-Gonzalez et al., 2019). However, high flow velocities hinder sediment trapping, or, in more extreme cases not modelled here, lead to erosion (Bosak et al., 2013). Conversely, low-energy settings with slow but non-zero water flow rates often prevent the healthy development of microbialites if mats are buried by muddy sediment (Johnson and Grotzinger, 2006; Andrews and Trewin, 2014; Curtis et al., 2021).

In Stromatobyte3D trapping and binding is calculated in two ways during each model iteration, once using an implicit calculation controlled by the input parameter g_{tb1}, hydrodynamic flow rate, and bathymetric slope, followed by a second calculation that explicitly accounts for the rate of trapping and binding of suspended sediment and potential poisoning effects based on the depositional rate of suspended sediment d_{susp} on each model grid cell. In the implicit calculation, sediment transport and agglutination from suspension into the microbial mat is not directly modelled at this stage of the model iteration for time step, but instead the implicit calculation represents vertical and lateral accretion by trapping of sediment into the sticky microbial mats and importantly, accounts for trapping over high slope gradients where suspended sediment would not normally be deposited (Kozlowski, 2016).

Modelled growth by precipitation and implicit trapping and binding includes both vertical and lateral growth. For a grid cell (x,y) with elevation h, each grid cell has a surface area determined by the cell size, and it can accrete material in one of the five directions $(z+, x+, x-, y+, y-)$, where $z+$ is vertical growth and the x and y variants are lateral growth. Lateral growth is calculated implicitly as a small-scale smoothing process that tends to reduce mound surface relief (Grotzinger and Rothman, 1996; Kozlowski, 2016), and it occurs when the elevation of a cell x,y is lower than any of the four adjacent cells. In this case, all of the higher cell(s) can accrete laterally into this central cell at different rates, depending on their own vertical growth rates. When the cumulative lateral accretion exceeds the

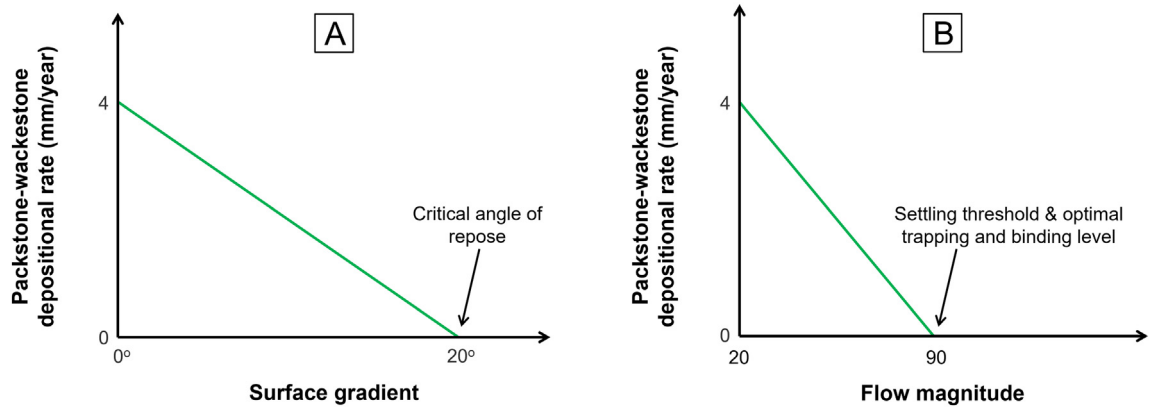

Fig. 2. (A) Linear relationship between topographic surface gradient and the maximum possible rate of packstone-wackestone deposition, following the simple approach used by Bitzer and Salas (2002) assuming no accumulation beyond the critical repose angle. (B) Relationship between flow magnitude and packstone-wackestone deposition. Higher water flux prevents settling of sediment from suspension, so rate of deposition from suspension goes to zero at a threshold flow magnitude, which is also the optimum flow rate for sediment trapping and binding. Rate of deposition from suspension is highest at the boundary flow magnitude, which is low but non-zero, hence able to transport suspended sediment across the model grid even as it settles out of suspension.

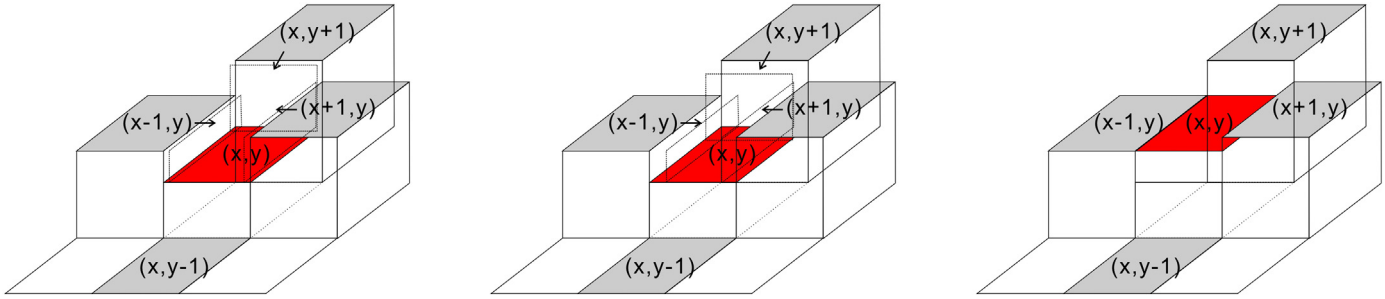

Fig. 3. Rationale of lateral and vertical growth in Stromatolite3D. Each cell can grow vertically, and lateral growth also occurs in the central cell in this case, because it is surrounded by three adjacent cells with higher elevation. As a result, they can accrete laterally and contribute to the vertical growth of central cell. The contribution of surrounding cells to lateral accretion is stored in a separate array. When the cumulative lateral accretion is above the cell size, the elevation of central cell will be increased up to the lowest neighbour cell.
Modified from Kozlowski (2016).

cell size, the elevation of this cell (h) will be increased up to the elevation of the lowest neighbour cell (Fig. 3).

2.3.2. Effect of hydrodynamics on implicit trapping and binding

For the implicit calculation, rate of microbialite growth due to trapping and binding is assumed to be proportional to the rate of deposition from suspension, controlled by flow magnitude M_{fm} which acts as a growth-rate modifier, following a symmetrically increasing then decreasing profile as flow magnitude increases (Fig. 4A). Growth rate is highest at the specified optimal trapping and binding level (Fig. 4A), representing the maximum rate of sediment input that can be captured and stabilised by the microbial community. It is assumed that a further increase of flow magnitude will decrease the mat's ability to trap passing sediment because the grains are moving too fast to be optimally trapped, or because the higher suspended sediment flux risks burying the microbial mat.

2.3.3. Effect of slope on microbialite trapping and binding

Although microbial mats can trap and bind sediment at high slope gradients, settling of sediment from suspension tends to accumulate in topographic lows, so the growth rate due to sediment trapping will be potentially increased in depressions. Another term affecting microbialite growth rate by trapping and binding (g_d) is used to represent the effects of slope on sediment trapping. Following the approach from Johnson and Grotzinger (2006), it is calculated using the second derivative of the bottom surface multiplied by a user-defined diffusion coefficient (k_{tb}, in m^2 per year):

$$g_{d(x,y)} = \frac{h_{(x,y-1)} + h_{(x,y+1)} - 2 * h_{(x,y)} + h_{(x-1,y)} + h_{(x+1,y)} - 2 * h_{(x,y)}}{d^2} * k_{tb} \quad (2)$$

where d is cell length, x and y are cell coordinates, h is elevation and k_{tb} is diffusion coefficient. As the value of k_{tb} increases, mound surface curvature at the previous time step will have a stronger control on the surface at this time step.

2.3.4. Microbialite growth by explicit trapping and binding and sediment poisoning

In the end of each time step iteration, if suspended sediment deposition and microbialite growth both occur in the same grid cell at this iteration, part or all of the suspended sediment will be trapped and directly incorporated into microbialite growth, depending on the threshold trapping and binding rate *tb*, which is an input parameter (Fig. 4B). Alternatively, if suspended sediment deposition exceeds 2*tb*, microbial mounds

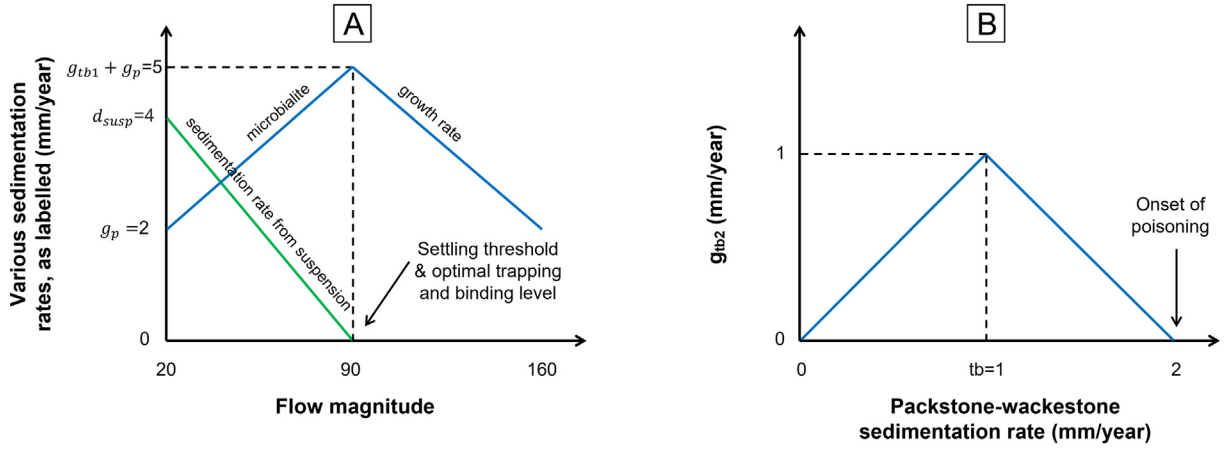

Fig. 4. (A) Relationship between flow magnitude on the horizontal axis, packstone-wackestone deposition from suspension (d_{susp}, green), and microbialite growth rate (g_p+g_{tb1}, blue) on the vertical axis. Precipitation rate is constant, while implicit sediment trapping rate is modified using a growth-rate modifier linked to flow magnitude M_{fm}. This relationship assumes that implicit trapping and binding and flow magnitude increase until the optimal trapping and binding level is reached, representing the maximum rate of sediment input that can be captured and stabilised by the microbial community. Further increase of flow magnitude will decrease the mat's ability to trap passing sediment. (B) Relationship between packstone-wackestone sedimentation rate d_{susp} and explicit trapping and binding rate g_{tb2}, when suspended sediment deposition and microbialite growth both occur in the same grid cell. If suspended sediment deposition d_{susp} is less than the threshold trapping and binding rate tb, all suspended sediment will be incorporated into microbialite growth, if $tb < d_{susp} < 2tb$, part of them will be incorporated. If $d_{susp} > 2tb$, mounds are smothered and buried by suspended sediment, recolonisation is required to recommence microbialite accumulation. (For interpretation of the references to colour in this figure legend, the reader is referred to the web version of this article.)

Table 1
Input modelled processes in four experiments, with increasing complex spatial feedbacks from experiments 1 to 4.

	1	2	3	4
Hydrodynamic model	No	Yes	Yes	Yes
Microbialite growth is flow magnitude dependent	No	Yes	No	Yes
Deposition of sediment from suspension is flow magnitude dependent	No	No	Yes	Yes

will be smothered due to sediment poisoning, so $R_{(x,y)} = 0$ and recolonisation is then required to recommence microbialite accumulation. Explicit trapping does not occur in cells if only occupied by one lithofacies.

2.4. Model cases and input parameters

Four models are run to understand how different modelled processes interact and what stratal patterns they can produce. Each model run is a numerical experiment to explore the consequences of one particular set of input parameters and modelled processes. The first experiment demonstrates a non-self-organized case with strong inheritance from the initial surface. Model elements are then progressively added in cases 2, 3, and 4, to explore how each additional factor controls the strata (Table 1). Input parameters are based on reasonable, constrained values used in previous study of marine microbial carbonate systems (Johnson and Grotzinger, 2006; Jahnert and Collins, 2012; Kozlowski, 2016; Curtis et al., 2021).

All four model cases use a 100 by 100 orthogonal regular model grid consisting of 10,000 data points in total. The grid point spacing is 0.5 m, so the total grid represents a 50x50m area. Initial topography (Fig. 5) is a smoothed random surface with synoptic relief up to 0.5 m, which is comparable to substrates in many modern and ancient microbialite systems (Coshell et al., 1998; Ginsburg and Planavsky, 2008; Coulson, 2016; Gallois et al., 2018). Each model time step is one year, and a total of 250 time steps yield 250 years of total elapsed model time (EMT). Initial water depth is 1 m, increasing through relative sea-level rise to 2.5 m in the end of model run.

Modern microbialites commonly have multiple phases of accumulation (Paull et al., 1992; Jahnert and Collins, 2012; Carvalho et al., 2018), and the averaged growth rate decreases with increasing time span of observation (Table 2) (Sadler, 1981; Schlager, 1999), so the input maximum growth rate is set to 5 mm per year, and a total of 250 years EMT can produce microbialites with height of approximately 1 m or less, consistent with observations from modern systems, such as Shark Bay (Playford et al., 2013), Bahamas (Dravis, 1983), and Bermuda (Gebelein, 1969). Maximum accumulation rate of suspended sediment is 4 mm per year, which is a reasonable rate for non-compacted sediment to be deposited and form packstones in marine settings.

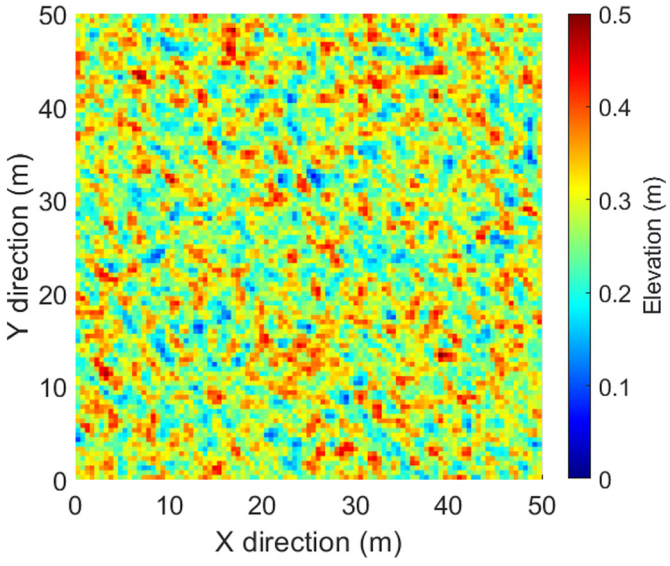

Fig. 5. Initial topographic surface used for all model runs. It is a smoothed random surface with maximum water depth of 1 m and synoptic relief up to 0.5 m.

3. Results

3.1. Experiment 1: isolated microbialite columns

In this simplest experiment, there is no hydrodynamic process modelled, sediment can still be transported in suspension, but hydrodynamics has no direct influence on accumulation of either modelled lithofacies. Since finer-grained sediment in suspension tends to inhibit and poison in-situ microbialite growth, microbialite nucleation and growth therefore occurs preferentially on stable topographic highs less than 2 m in width where sedimentation rate from suspension is lowest because of the higher topographic gradients. Reduced poisoning and burial from suspension leads to increased mat accretion and survivability. In contrast, growth is inhibited in topographic lows where a higher sedimentation rate suppresses and overwhelms microbial growth (Johnson and Grotzinger, 2006; Della Porta, 2015; Baskin et al., 2021). Results of experiment 1 show many distinct isolated small microbialite columns, about 1–1.5 m in width and less than 1 m in height scattered across the model surface in a visually random distribution (Fig. 6). In planform, the spatial distribution and geometry of these mounds is predominantly inherited from the distribution of high areas on the initial surface, with no preferred orientation. This strong substrate control can be also seen in cross section (Fig. 7), where most of the mounds are growing on top of initial topographic highs; percentage of surface points occupied by actively growing and accreting mats at the end of model run indicates that, microbialite areal coverage in experiment 1 is only 13.78% (Table 3).

3.2. Experiment 2: elongated microbialites

A dominant flow direction is imposed in experiment 2, from the bottom of the grid towards the top. In comparison to experiment 1, microbial mounds preferentially nucleate, either on narrow steep-gradient topographic highs where only limited amount of suspended sediment can accumulate, or on the margins of broad antecedent topographic highs or previous build-ups where flow magnitude is relatively high. The latter creates some spatial interactions between topography, hydrodynamics, and mat accretion, which creates some relatively large build-ups because subsequent growth preferentially occurs next to pre-existing microbial mounds. Aligned mounds are mostly several meters long, some can grow up to 8 m, apparently elongated and aligned in the defined current direction (Fig. 6). Some microbialites have composite forms in planform due to lateral accretion and coalescence (Fig. 7). As well as elongated mounds, these growth patterns also lead to some relatively large gaps between microbial mounds that do not simply reflect the underlying initial topography; topographic highs in these areas have been buried rather than growing mounds. There are still many small and isolated mounds, similar to experiment 1, but the overall microbial mound distribution shows an increased degree of clumping and coherency, total microbialite volume percentage is lower, areal coverage is increased by 1.42% relative to experiment 1 (Table 3), and the dependence of mound growth on initial condition is reduced.

Table 2
Holocene microbialite growth rates on average in various locations and settings. Note that averaged growth rate decreases as the observational time span increases due to the Sadler effect.

Location	Growth rate (mm/year)	Time span (years)	Setting	Reference
Whale Bay, Bermuda	Up to 3 mm per day	–	Marine	(Gebelein, 1969)
Laguna Bacalar, Mexico	Up to 10	20	Lacustrine	(Kozlowski, 2016)
Lake Clifton, Australia	0.95–1.55	250–430	Lacustrine	(Parellada, 2016)
Shark bay, Australia	0.10–0.54 Locally up to 3	295–1760 Locally only 20	Coastal marine	(Jahnert and Collins, 2012)
Lagoa Salgada, Brazil	0.10 on average	–	Lacustrine	(Bahniuk, 2013)
Lagoa Vermelha, Brazil	0.09–0.54 0.19 on average	~450	Lagoon	(Carvalho et al., 2018)
San Salvador, Bahamas	0.16 on average Up to 0.88	2310	Lagoon	(Paull et al., 1992)

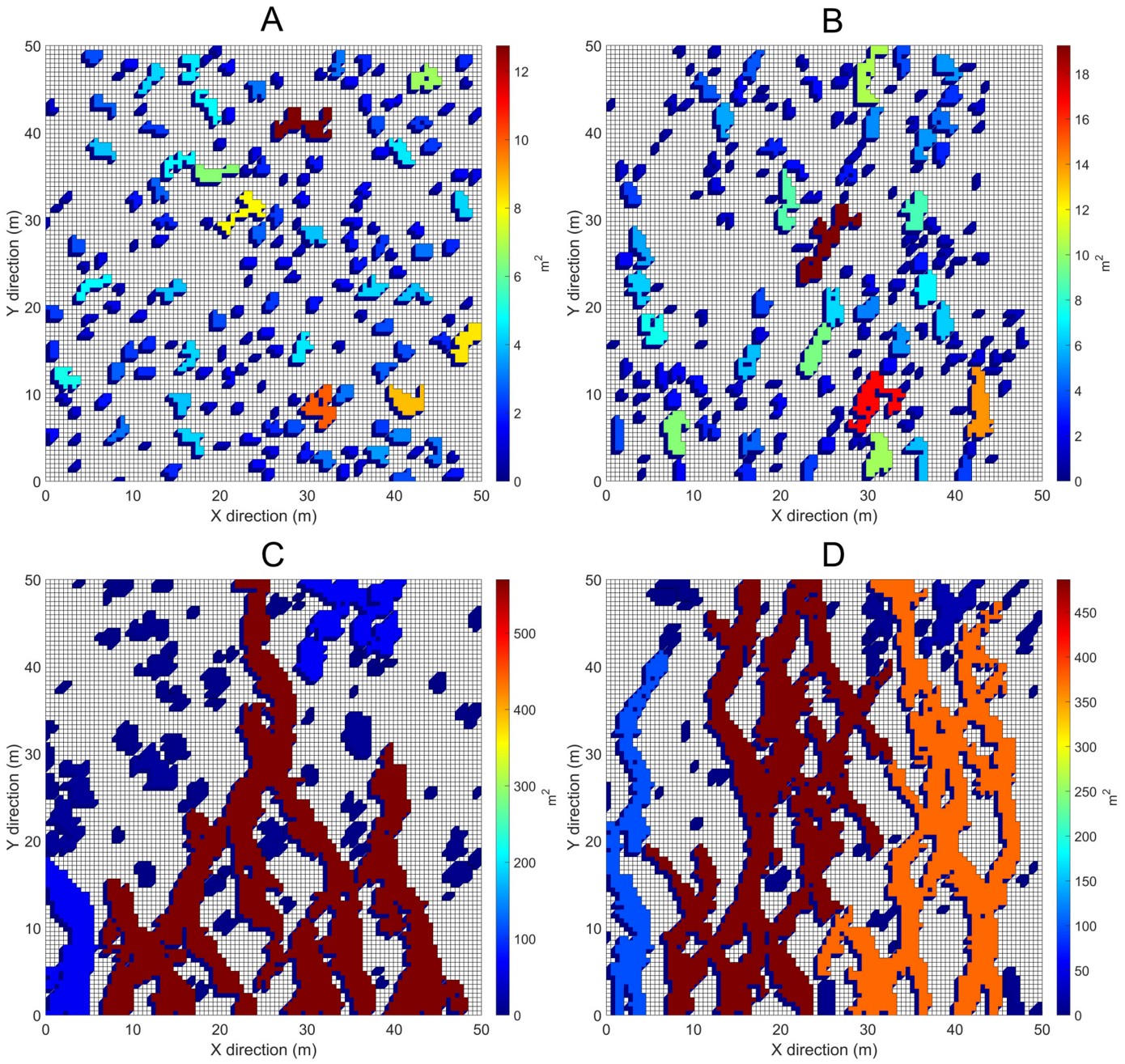

Fig. 6. Map view of the model grids from the four experiments after 250 years elapsed model. Microbial accumulations are colour coded in terms of their 2D connected areas in m2. Related statistics for each experiment are listed in Table 3. With the exception of experiment 1, water flow direction is from the bottom to the top of model grid. Note increasing mound connectivity from small, isolated columns in experiment 1 (A), through composite and elongated shapes in experiment 2 (B), to well-connected ridges parallel to flow direction in experiments 3 (C) and 4 (D). Substrate topography is a deterministic control in experiment 1, but this control is progressively weakened in experiments 2 to 4, due to the potentially self-organizing spatial feedbacks. (For interpretation of the references to colour in this figure legend, the reader is referred to the web version of this article.)

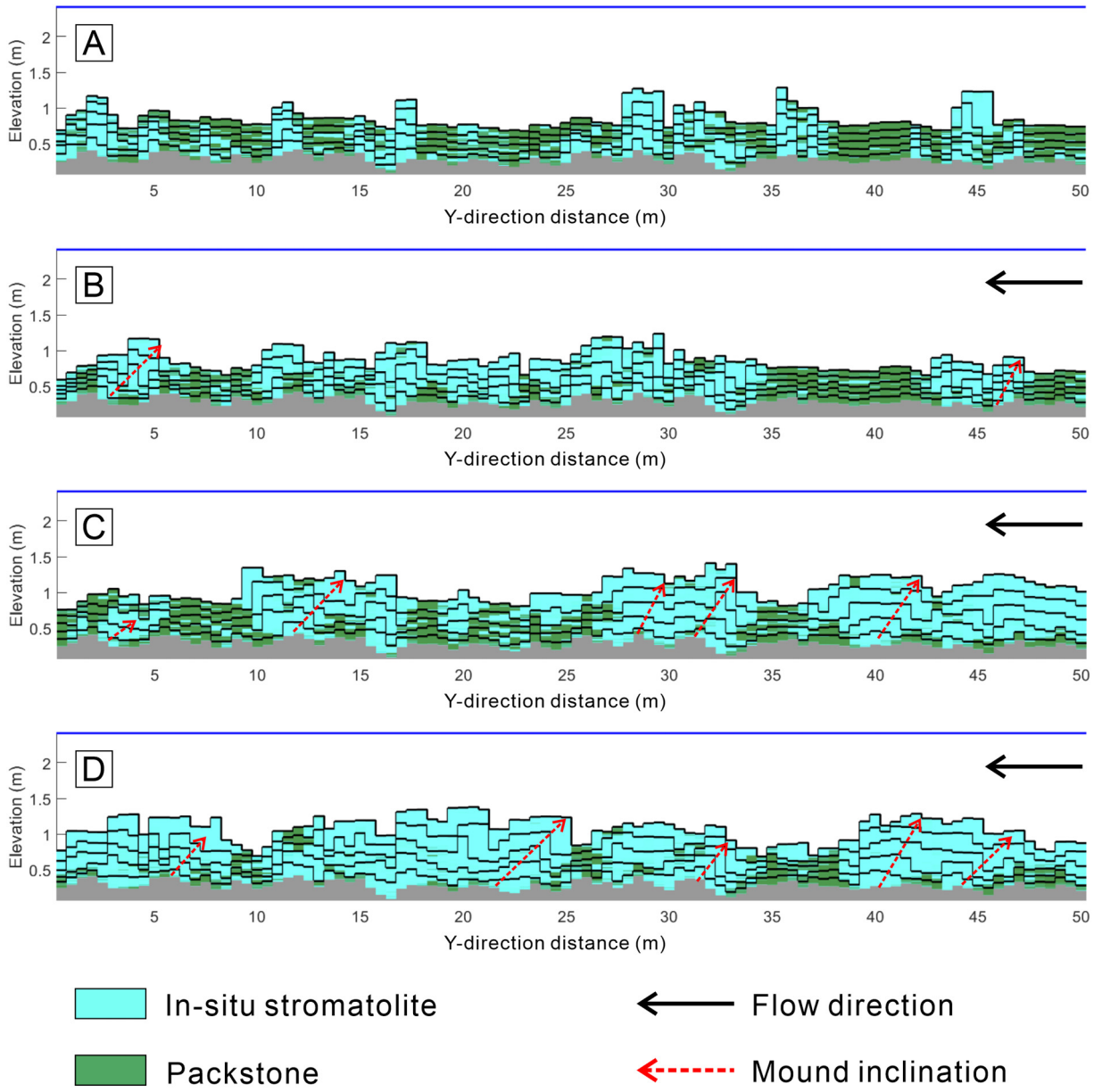

Fig. 7. Cross sections from the four experiments at X = 25 m, parallel to input flow direction. Horizontal black lines represent timelines at 50 year increments. Experiment 1 (A) has no flow direction, microbialites are narrow, steep, and primarily grow vertically, mostly from initial topographic highs. In experiment 2 (B), microbialites start to grow and expand laterally, and some are inclined towards the flow direction because accretion is faster on the windward sides. In experiments 3 and 4, laterally adjacent microbialite columns coalesce due to rapid lateral growth. This lateral coalescence causes a progressive increase of microbialite lithofacies proportion in these flow-parallel sections from experiments 1 to 4, while the actual microbialite volume percentages (Table 3) do not change significantly. The result in experiments 3 and 4 shows a strongly preferred orientation with the development of ridges and runnels.

3.3. Experiment 3: microbialite ridges and Y-junctions

In experiment 3, calculated water flow magnitude is a control on the rate of packstone sedimentation from suspension, but not directly on the microbialite growth rate. This weakens the influence of substrate topography on sedimentation rate compared to experiments 1 and 2. Sedimentation from suspension preferentially occurs in tranquil areas where flow magnitude is relatively low, and because suspended sediment inhibits and 'poisons' in-situ microbialite growth, mound survivability is higher where flow magnitude is high. Consequently, microbialites in this experiment are much more elongated and well-connected than experiment 2, forming microbialite ridges across the entire model grid, separated

Table 3
Statistics of four model experiments, including lithology volume percentages, microbialite areal coverage, maximum and mean mound area in planform.

	Experiment 1	Experiment 2	Experiment 3	Experiment 4
Microbialite vol%	51.4	47.9	57.1	52.9
Packstone vol%	48.6	52.1	42.9	47.1
Areal coverage (%)	13.78	15.20	35.45	42.16
Maximum area (m^2)	13	19	570	487
Mean area (m^2)	1.45	1.38	5.47	5.04
2D connectivity	0.5496	0.6472	2.2208	2.6284

by packstone-covered runnels (Fig. 6). The ridges are subparallel to each other, elongated parallel to input flow direction, and extend across a significant portion of the entire model surface. Some ridges develop 'Y-shaped' junctions, opening in the direction of flow, where two adjacent mounds accrete and migrate laterally, eventually leading to downstream coalescence. Microbialite areal coverage is increased by 20% and volume percentage by 9% relative to experiment 2. Despite this control by flow magnitude, there are still some persistently accumulating small mounds located over topographic highs on the initial surface. In cross section, because many microbialites can trap and incorporate suspended sediment, they expand laterally and prograde over adjacent sediment (Fig. 7). The stromatolite strata are inclined, with bedding surfaces dipping in the flow direction, and faster accretion rates facing up-current.

3.4. Experiment 4: ridges and runnels

Experiment 4 has the most complex model formulation and strongest spatial feedbacks between model components. Flow magnitude determines rates of both in-situ growth and sedimentation from suspension, which in turn modify topography and the spatial distribution of flow magnitude. Topography-flow-sedimentation interactions create a well-organized 'ridge-and-runnel' pattern across the entire model surface, elongated parallel to flow direction (Fig. 6). Lateral growth and coalescence of adjacent stromatolites is most common and prevalent in this experiment (Fig. 7), isolated mounds rarely occur (Fig. 6). Such strong mound elongation with rapid accretion only in the flow direction explains the absence of 'Y-shaped' junctions because lateral accretion perpendicular to the flow direction is significantly suppressed in this more strongly directional hydrodynamic setting. Microbialite growth is no longer controlled by initial topography because the microbialite ridges generate strong feedbacks between flow, sedimentation, and topography as they develop and adjust their positions. Formation of coherent ridge patterns, produced by spatial feedbacks, and independent of initial condition, is evidence of spatial self-organization. These patterns also significantly increase the microbialite areal coverage to 42%, though the total volume percentage in this experiment is actually lower than experiment 3, and very close to experiment 1. This contradiction is due to strong upward-expansion of microbialite growth as microbialites expand their top surfaces over underlying old laminae (Figs. 7 & 11).

3.5. Comparison with modern Shark Bay stromatolites

Modelled microbialites are compared with modern agglutinated stromatolites in Hamelin Pool, Shark Bay, Australia. Jahnert and Collins (2012) provided a detailed substrate map with bathymetry data (Fig. 8). Playford et al. (2013) conducted a regional geological survey of Shark Bay with many useful field and aerial photos to show different stromatolite structures and their distributions around the margins of Hamelin Pool. The study includes both the well-known locations on the eastern and south-eastern margins, and various locations on the west margin that have not previously been studied and reported. Based on high-resolution mapping and extensive in-water observations, Suosaari et al. (2016) recognised several distinct 'stromatolite provinces' around the margins of Hamelin Pool, each with characteristic morphologies, geographic distribution, and substrate gradient. These previous studies provide important information and data that allow a comparison between this model and field observations.

Modelled microbial mounds are strikingly similar to observed stromatolite morphologies (Fig. 9). Classic individual stromatolite columns in experiment 1 correspond to the Flagpole Province in the southeast, where substrate gradient is relatively gentle. Stromatolite heads can merge occasionally. The elongated form of stromatolites in experiment 2 are referred to as 'longitudinal stromatolites' by Playford et al. (2013), they also have composite forms due to aggregation of adjacent stromatolite heads. They can be found in the Carbla Province on the eastern margin and the Spaven Province on the western margin. Stromatolite ridges in experiments 3 and 4 can be found on the south-western margins, near Booldah well, where they are north-south oriented, parallel to prevailing wind direction. They are also referred to as seif structures (Playford et al., 2013), separated by bare sandy areas, some develop Y-junctions opening to the south (Fig. 8). Playford et al. (2013) also noted that some stromatolites in the south of Carbla Point are apparently inclined towards

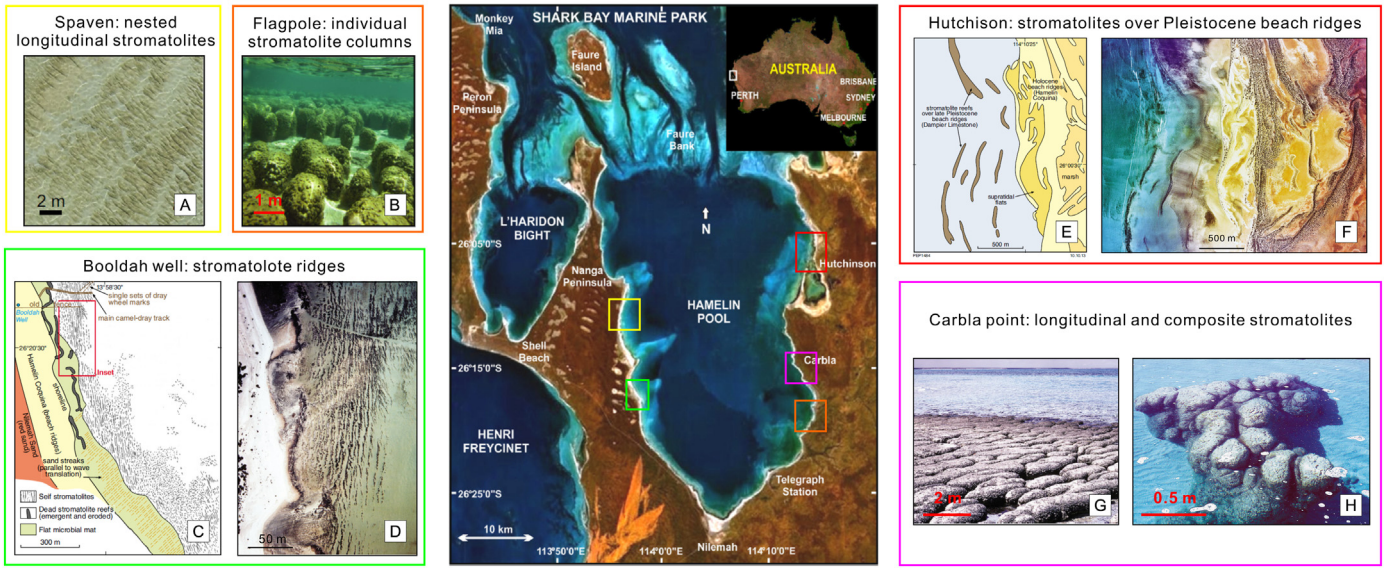

Fig. 8. Map of Hamelin Pool, Shark Bay, West Australia, shows five mapped stromatolite provinces with morphologically distinct structures around the pool margins according to Suosaari et al. (2016). Spaven Province (yellow box, A) is characterised by extensive subtidal stromatolites, they are elongated individually parallel to the wave direction, and their large-scale nested structures are directly controlled by the underlying Pleistocene beach ridges. Booldah well Province (green box, C and D) is characterised by a prominent pattern of stromatolite ridges oriented north-south parallel to prevailing wind direction. They are also referred to as seif stromatolites, usually tens of meters long, and can develop Y-shaped junctions open in the flow direction. Flagpole Province (orange box, B) is characterised by classic discrete stromatolite column, stromatolite heads can sometimes merge. Carbla Province (magenta box, G and H) is characterised by extensive longitudinal stromatolites, elongated parallel to wave direction. Some develop composite forms due to aggregation of adjacent stromatolites. Hutchison Province (red box, E and F) is somehow similar to the Spaven Province, and it is characterised by elongated stromatolites growing on top of Pleistocene beach ridges that can extend for hundreds of meters. (For interpretation of the references to colour in this figure legend, the reader is referred to the web version of this article.)
Images in A, B from Suosaari et al. (2016), images in C, D, E, F, G, H from Playford et al. (2013), substrate map from Jahnert and Collins (2012).

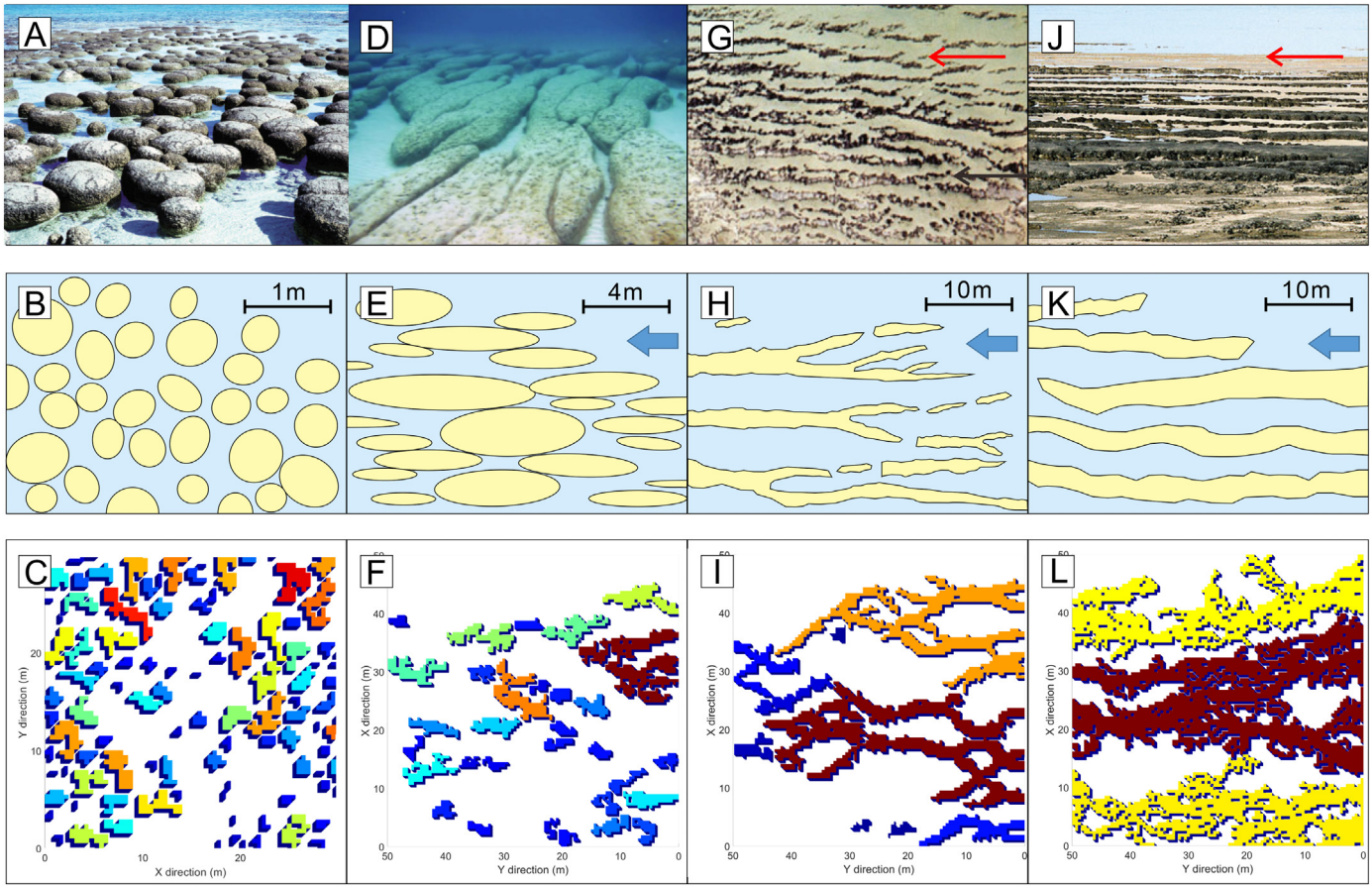

Fig. 9. (A–C): Classic isolated stromatolite columns, including a field photo in the southeast coast of Hamelin Pool, Shark Bay, passing from dead stromatolite tops in the foreground, to dark-brown living forms in the middle, and shallow subtidal forms in the background. (A), a cartoon illustration (B), and a selected model example of experiment 1 (C). (D–F): Longitudinal stromatolites elongated in the direction of flow, including field observation in Spaven Province, a simplified carton to illustrate the wave impact (E), and a model example of experiment 2 (F). Note the composited form of some mounds in both field observation and model output due to lateral mound coalescence. (G–I): Elongated stromatolite ridges subparallel to each other. Note two adjacent mounds can accrete sediment laterally, leading to downstream coalescence to produce 'Y-shaped' junctions, opening in the direction of flow. This is observed in Booldah Province (G), illustrated in (H) and reproduced in model (I). This selected example of experiment 3 shows merging of microbialite ridges in the flow direction from 11 heads on the right to only three heads on the left. (J–L): Stromatolites ridges parallel to the flow direction, separated by bare sandy runnels, in Booldah Province, from Playford et al. (2013), this coherent pattern is also shown in (K), and replicated in the model (L).
Images in (A, G and J) from Playford et al. (2013), image in D from Suosaari et al. (2016).

prevailing wind direction, resulting from rapid accretion of a mixture of carbonate and siliciclastic sand particles on the side exposed to up-current flow. These elongated forms with asymmetric features are also observed in Bahamas (Dravis, 1983; Dill et al., 1986), Bermuda (Gebelein, 1969), and are consistent with our modelling results (Fig. 7).

3.6. Comparison with ancient outcrop observations

Given the modelling results and the striking visual similarity to modern microbialite depositional systems, an important question is how model results compare to ancient strata. Many previous studies have highlighted the difference between modern and ancient microbialites in their shape, size, fabric, and accretion processes, due to long term evolution of microbial mats and environmental changes (Grotzinger and Knoll, 1999; Reid et al., 2000; Riding, 2011b). Ancient elongated stromatolite morphologies are rare, with a few exceptions, such as those Early Proterozoic examples on the shore of Great Slave Lake, North West Territories, Canada (Hoffman, 1974), and Middle Old Red sandstone sequence of Orcadian Basin, Scotland (Andrews and Trewin, 2014). Coulson (2016) studied a 13 m-thick vertical succession of subtidal microbialites in western Utah, US, which provides a useful ancient analogue to be compared with this model and modern observations above. He found this upper Cambrian succession shows a symmetric trend in terms of sediment grain size and microbialite length (Fig. 10), passing from fully detached round to ellipsoidal forms at the base, to slightly elongated and aligned forms, and well developed large microbialite ridges in the middle of succession. Then ridges retrograded back to slightly elongated forms and eventually to small, isolated forms at the top. This succession is interpreted to record a progressive increase of hydrodynamic energy with increasingly strong influence on sedimentation patterns to facilitate lateral accretion and coalescence to develop elongated microbialite ridges (Coulson, 2016), as we see from experiments 1 to 4. Ridge formation is followed by the exactly opposing trend, as accommodation increases, the hydrodynamic influence on sedimentation patterns becomes progressively weaker, and eventually current action is minimal at the top of succession.

4. Quantitative analysis of modelled microbialite geometries

4.1. Evolution of growth and suspended sediment deposition

Microbialite morphologies are fundamentally controlled by both growth and adjacent sedimentation rates, and these can exhibit complex spatial and temporal evolution (Grotzinger and Rothman, 1996; Grotzinger and Knoll, 1999; Della Porta, 2015; Curtis et al., 2021). Both rates can be measured in Stromatolite3D (Fig. 11). Many qualitative interpretations of outcrops and related depositional models suggest a balance between growth and sedimentation developing after a certain time, but

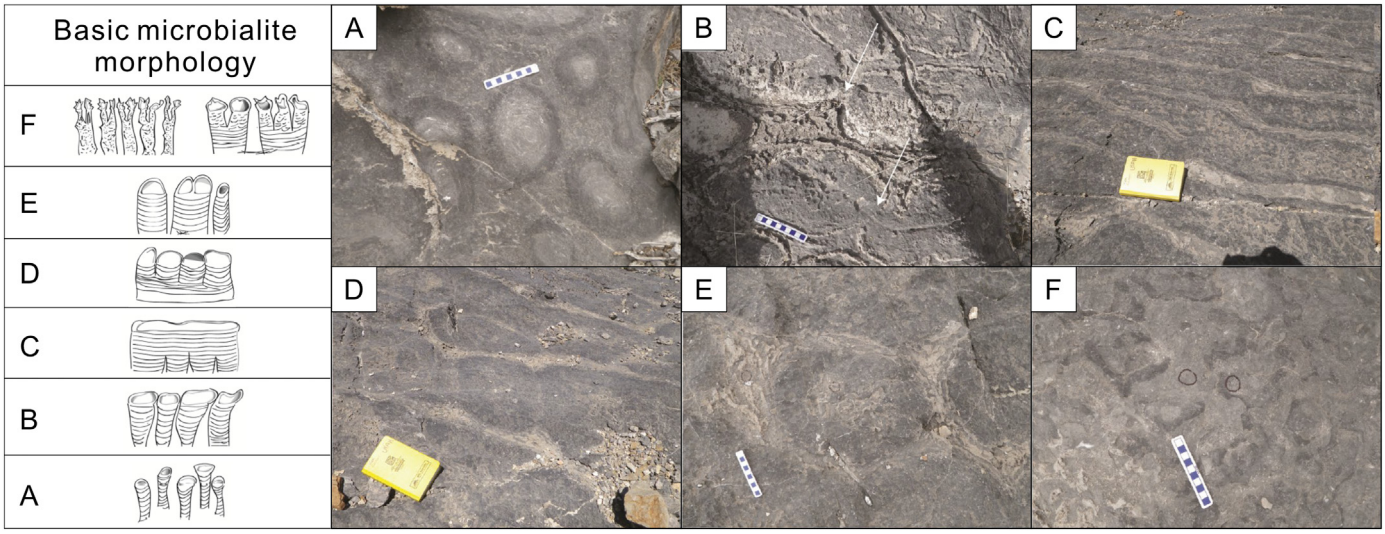

Fig. 10. Six distinct microbialite morphology seen in planform, moving up-section from the base to the top of a 13 m-thick vertical succession of Notch Peak Formation of western Utah. These morphologies can be correlated across 30 km^2. (A): Isolated, cm-scale round to ellipsoidal forms located at the base. (B): Slightly elongated forms, white arrows indicate suture zones of incipient alignment and lateral coalescence. (C): Meter-scale microbialite ridges with strong orientation and alignment, note these ridges are narrow with smooth edges. (D): Elongated forms start to detach and become wider. (E): Fully-detached dm-scale round forms. (F): Isolated, cm-scale sub-round to irregular forms at the top. Modified from Coulson (2016).

none of the four experiments shows any evidence for such equilibrium being reached. In experiment 1, microbial growth is progressively restricted and buried by adjacent onlapping sediment, and mounds show a transition from aggradation to retrogradation in cross section (Fig. 7). The other three experiments show exactly the opposite trend, with fast in-situ growth dominating, so mounds prograde and amalgamate laterally, and inter-mound sedimentation becomes more spatially restricted through time. Interestingly, the highest mound planform coverage seen in experiment 4 is not just due to higher growth rate, because growth rate in experiment 4 is lower than experiments 2 and 3. This apparent contradiction suggests an operation of some more complex processes, most likely an element of spatial self-organization, perhaps similar to the modern reticulate reef patterns (Purkis et al., 2015; Schlager and Purkis, 2015), or to modern mussels beds that generate regular ridges with erosion by tidal flows in between (Rietkerk and van de Koppel, 2008). In that case, spatial feedbacks between in-situ growth rate and deposition from suspension lead to mound growth optimised along ridges parallel to waves and tidal currents. Isolated mound growth is less optimal for it to survive, so it is rare in a mature and more organized system, such as experiment 4, but still present in experiments 2 and 3 where spatial feedbacks are less developed.

4.2. Dependence on initial surface: topography correlation coefficient (R)

Dependence of microbial mound growth on initial topography is analysed quantitatively to test these interpretations of self-organization. If these mounds are self-organized, their occurrences and positions should be independent of initial surface topography. A new metric, topography correlation coefficient (R), is constructed and used to quantify the degree of dependence on initial surface. It is simply defined as the proportion of the highest 20% of the points on the initial surface that persist as high points on the final surface (Fig. 12). Nearly half of the mounds in experiment 1 grow directly on initial highs. Experiment 2 represents a transitional case where the initial surface still determines some of the microbialite occurrences, but interaction between mound growth and hydrodynamics allows lateral accretion to develop longitudinal mounds, causing a decrease of R to 0.310. The final two experiments both develop microbialite ridges, with R values around 0.250, suggesting a very weak dependence on the initial surface. It is important to note that R values cannot be zero, because high points on the initial surface are randomly distributed, and even if these is no causal link between initial and final high points, some elevated points on the final microbialite surface will always be coincidental to initial topographic highs due to upward-expansion of microbial mounds.

The sensitivity of the high points criteria to the selected proportion of highest points on the initial surface is also tested, and the results show that with high point proportions ranging from 5 to 15%, this new metric can clearly distinguish the strongly substrate-controlled example in experiment 1 with the more laterally-expansive and potentially self-organized examples in experiments 2–4 (Fig. 12). However, the transitional nature of experiment 2 is more apparent when more than 15% of the highest points are selected, so we used a default of 20% in the four experiments.

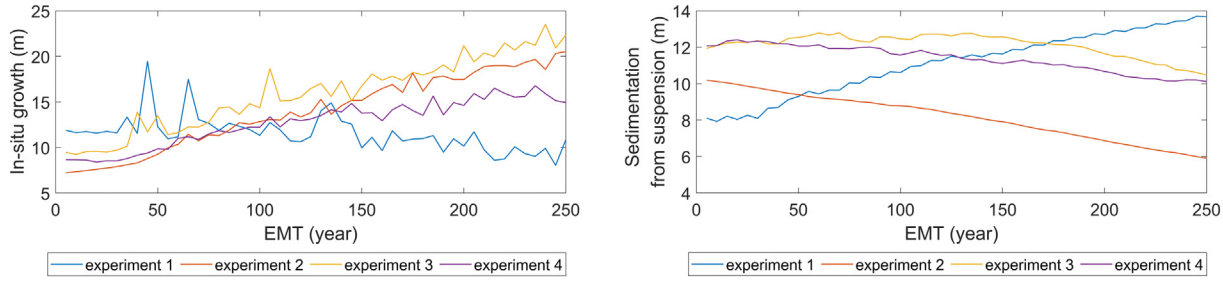

Fig. 11. Evolution of accumulated in-situ and suspended sediment of four experiments. Note none of the four experiments has reached a dynamic equilibrium state. Mounds in experiment 1 are progressively buried by increasing sedimentation from suspension. The remaining three experiments show the opposite trend, due to the effects of lateral accretion and coalescence causing upward-expansion of top surface.

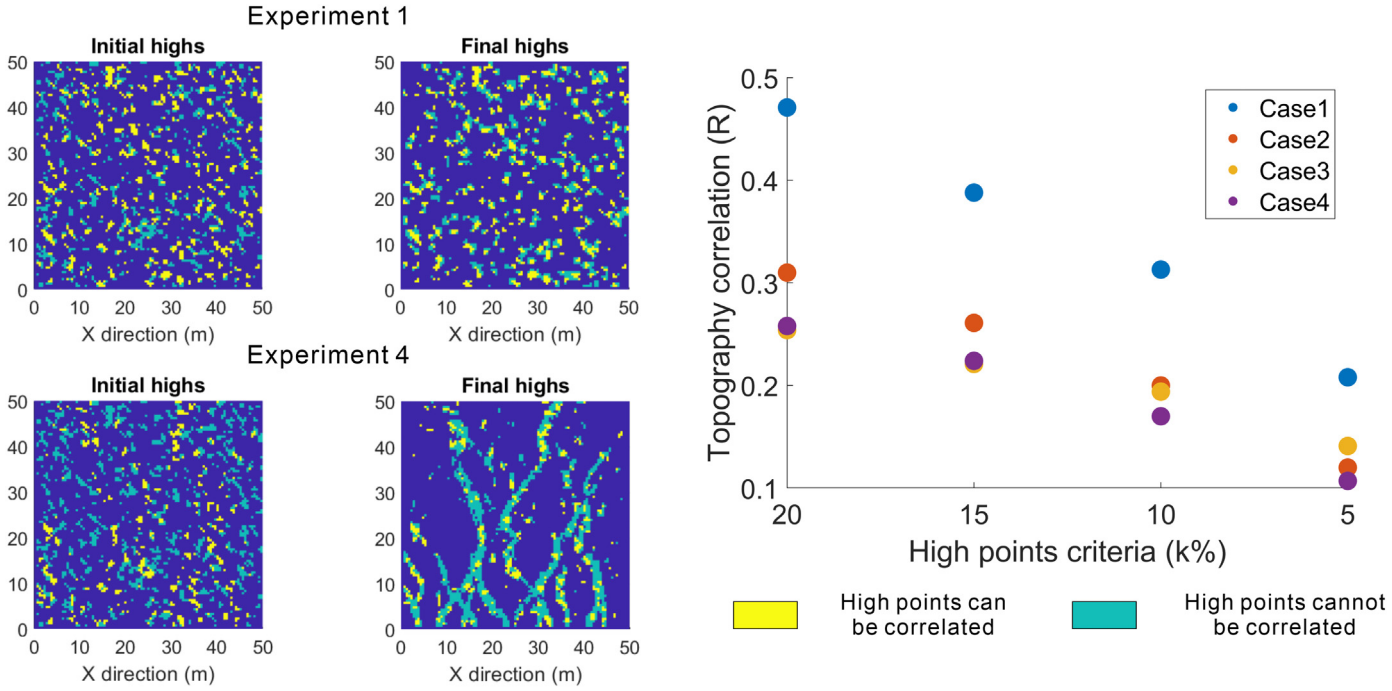

Fig. 12. Left: how initial topographic high points persist as final topographic highs in experiments 1 and 4. Note nearly half of final high points (47.1%) can be correlated to initial high points in experiment 1, but this percentage is a much lower (25.8%) in experiment 4. Right: the sensitivity of the high points criteria to the selected proportion of highest points on surface, this plot shows that this metric is also useful and valid for high point proportions of 15%, 10% or 5%.

4.3. Evolution of surface roughness and irregularity

Microbialite growth is a dynamics process of mat accretion alternating with periods of sediment deposition from suspension (Grotzinger and Knoll, 1999). Growth on microbial mats tends to produce an irregular, rough surface but settling of sediment out of suspension tends to fill in local depressions and effectively smooths the surface. One might expect the various interactions of these two processes to generate varying degrees of surface roughness and irregularity, and this is investigated here using Stromatobyte3D.

Surface roughness can be measured as the deviation of the height of individual surface point from the mean surface height, following the definition by Barabási and Stanley (1995);

$$w(L,t) = \sqrt{\frac{1}{L}\sum_{i=1}^{L}\left[h(i,t) - \overline{h}(t)\right]^2}$$

where L is the total number of points, h is the height for any point on this surface, t is time step, i is an index number, and $\overline{h}$ is the mean surface height. An 'in-situ growth-dominated' system with a higher volume percentage of microbialite will generally have rougher surfaces, so experiment 3 has the highest roughness (Fig. 13). In contrast, a 'sedimentation from suspension-dominated' system like experiment 2 has the lowest roughness. Surface roughness in experiment 1 increases very slowly after 160 years, because localised growth on initial topographic highs cannot be sustained, so sedimentation from suspension gradually dominates and smooths the surface (Figs. 11 & 13). Surface roughness evolution in experiment 4 is almost identical to experiment 3, suggesting better developed ridges and runnels due to more lateral amalgamation can maintain surface roughness even when stromatolite volume is reduced.

Many modern microbialites are associated with elevated polygonal structures (Coshell et al., 1998; Bouton et al., 2016), or vegetation (Gallois et al., 2018), because an irregular and wavy surface has a higher 'seeding potential' and therefore facilitate microbialite growth. Surface irregularity is calculated as the percentage of bump points on the modelled topographic surface at every time step, following the definition by Leach (2014). A point will be considered 'bumpy' when the average height differences between this point and four adjacent points is above a threshold value, in this case 0.03 m. Evolution of surface irregularity in the four experiments (Fig. 14) are very different from the previous surface roughness plot. Isolated mounds give experiment 1 the highest irregularity with an increasing trend through time, associated with a transition from mound aggradation to retrogradation as growth rate decreases (Fig. 11). Surfaces are most regular in experiment 4 with little fluctuation, in contrasting to their surface roughness which

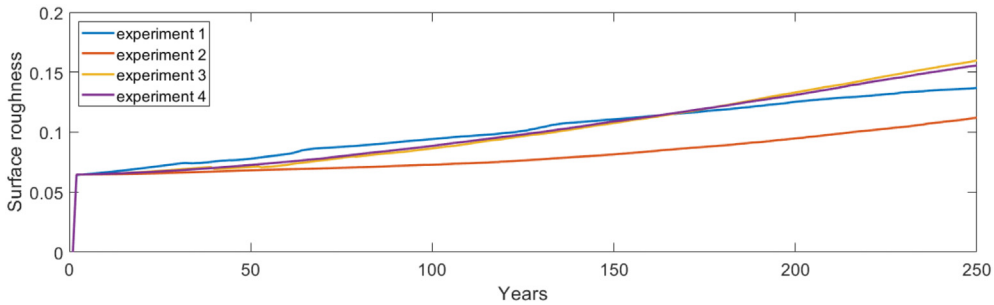

Fig. 13. Surface roughness evolution of four experiments.

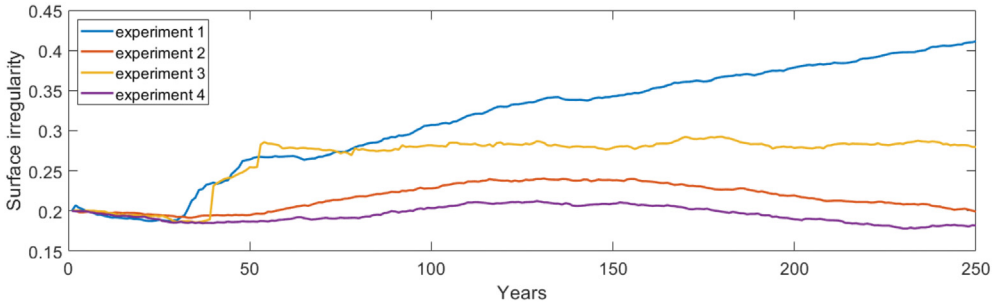

Fig. 14. Evolution of surface irregularity of four experiments.

is highest of the four experiments (Fig. 13). This contrast reflects the development of 'ridge and runnel' patterns. Ridge crests elevate faster than the mean surface elevation increases, so surface roughness increases. Conversely, these ridges are spatially extensive with flat tops, so their growth reduces surface irregularity. Ridges are not developed in experiment 2, but the smoothing effect due to high sedimentation from suspension helps to maintain surface regularity (see Table 3). Quantifying surface characteristics and evolution is complicated because surface geometry tends to be complicated, but by coupling two quantitative metrics here, these results show how the dynamics of microbial mound morphology are controlled by interactions of opposing depositional processes.

4.4. Connectivity

Microbialite strata can be important reservoirs for hydrocarbons, stored CO_2, or other fluids, so it would be useful to characterise and understand their connectivity, and their connectivity could also perhaps be another metric to distinguish self-organized examples. A simple algorithm is developed to quickly calculate 2D connectivity from a map-view surface in the end of model run. For each cell on the final surface occupied by microbialite, adjacent cells also occupied by microbialite are counted as connected. Both diagonally and orthogonally adjacent cells are counted. The sum of this count is divided by the total number of grid cells to yield an estimate of gross planform connectivity (Fig. 15). Increasing gross connectivity is observed from experiments 1 to 4, consistent with their large-scale morphologies. This suggests that stronger spatial feedbacks between depositional system components will lead to mound coalescence and in turn enhance connectivity in microbialite strata, with potentially very significant implications for understanding subsurface reservoir connectivity.

5. Control by an organized substrate

The nature of the substrate is considered as an important control on microbialite nucleation and growth. Stromatolite growth usually requires a stable and rocky substrate rather than soft mud or mobile ooidal sand (Logan et al., 1974; Andres and Reid, 2006; Ginsburg and Planavsky, 2008; Della Porta, 2015). In Shark Bay, stromatolites are generally better developed around headlands where local Pleistocene beach ridges and Miocene quartzite outcrops form suitable indurate substrates (Playford et al., 2013). Experiments 1 to 4 demonstrate how self-organization creates ordered morphology and strata from a disordered initial topography, but an outstanding question is what patterns will be produced if the substrate itself is highly organized with regular morphological features? In order to address this question, a new initial surface is used with several evenly-spaced linear ridges, each with relief up to 0.5 m, representing antecedent beach ridges as observed in Shark Bay (Fig. 16). Two additional experiments are conducted, equivalent to experiments 1 and 4 except for the different initial surface. These two experiments are referred to as experiments 1b and 4b.

Microbialite occurrence is strongly controlled by the underlying substrate in experiment 1b (Fig. 17), where growth is limited to initial substrate highs (Table 4). Rapid sedimentation from suspension inhibits growth in the remaining area where topography is flat. Consequently, both microbialite volume percentage and areal coverage reduce dramatically compared to experiment 1 (Table 4). In cross section, there is a trend from aggradation to retrogradation, as stromatolite columns are gradually buried by adjacent packstone. Parallel to the flow direction, substrate highs are wider, stromatolites grow over the entire ridges initially, then split into columns as they grow vertically, developing compound morphologies. The area directly above the top of initial surface highs is not as steep as the flanks so sedimentation from suspension will be faster though time, and eventually creates a topographic saddle (Fig. 17).

The substrate control is still very strong in experiment 4b, but to a lesser degree compared to experiment 1b (Table 4). A major difference in this case is the increasingly closer spatial feedbacks that facilitate rapid sediment trapping and lateral growth, so mounds can expand and prograde in the flow direction (Fig. 17). Consequently, mounds extend further than the initial topographic highs. Many relatively small mounds are nucleating on the windward side, which can potentially interact and be amalgamated with existing large mounds. Compared to experiment 4, microbialite volume, areal coverage, and connectivity in experiment 4b are much lower due to stronger dependence of substrate. This experiment might represent a hybrid and transitional case, similar to the Spaven Province and Hutchison Province in Shark Bay, where individual stromatolite growth can respond to local hydrodynamic conditions with direction of elongation parallel to flow direction, and their large-scale nested distribution is primarily controlled by the underlying Pleistocene beach ridges (Playford et al., 2013; Suosaari et al., 2016).

6. Discussion

The concept of self-organization and how it works comes originally from the classic 'reaction-diffusion' model (Turing, 1952). In his model, local feedbacks occur between reaction components, but spatial information is also transmitted over a longer distance via diffusion. Formation of stable patterns requires the diffusion rate of inhibitor to be faster than the activator. Since both the Turing model and Stromatobyte3D generate patterns through self-organization, it is useful to compare both models. Microbialite growth occurs locally as the activator, inhibited over longer distances by the background packstone deposition from suspension. In experiment 4, in-situ growth and sedimentation from suspension both control and are controlled by topographic evolution and associated flow magnitude. As a result, patterns in Stromatobyte3D emerge due to the interaction of topography, hydrodynamics, and two types of sedimentation, with positive feedback dominating at short scale and negative feedback dominating at the larger scale, so very similar overall to the original activator-inhibitor model from Turing (1952).

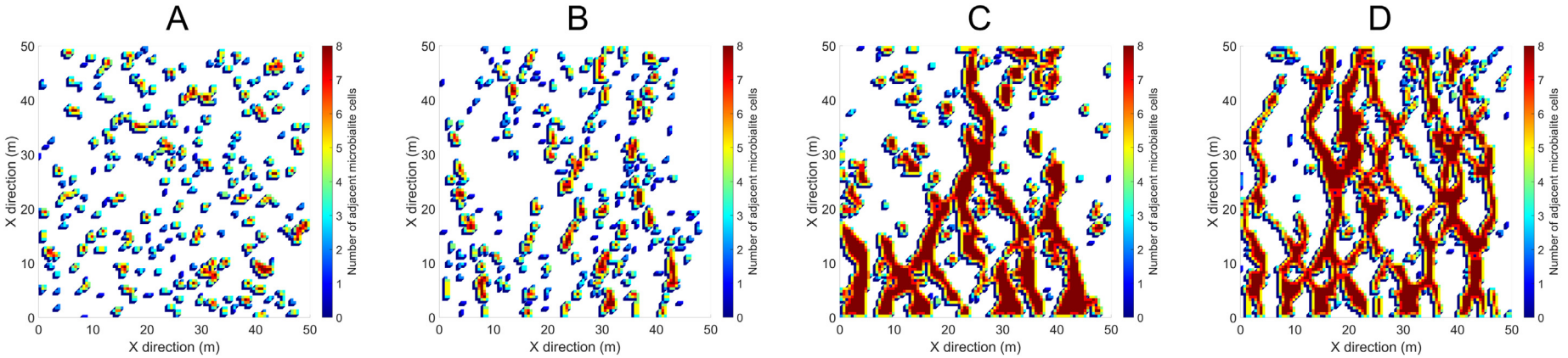

Fig. 15. 2D connectivity of four experiments. Each cell occupied by microbialite can be connected to up to 8 adjacent microbialite cells. Connectivity values are listed in Table 3, exhibiting an increasing trend from isolated columnar shape in experiment 1, through longitudinal shape in experiment 2, to ridges and runnels in experiments 3 and 4, from, as the spatial feedbacks become stronger.

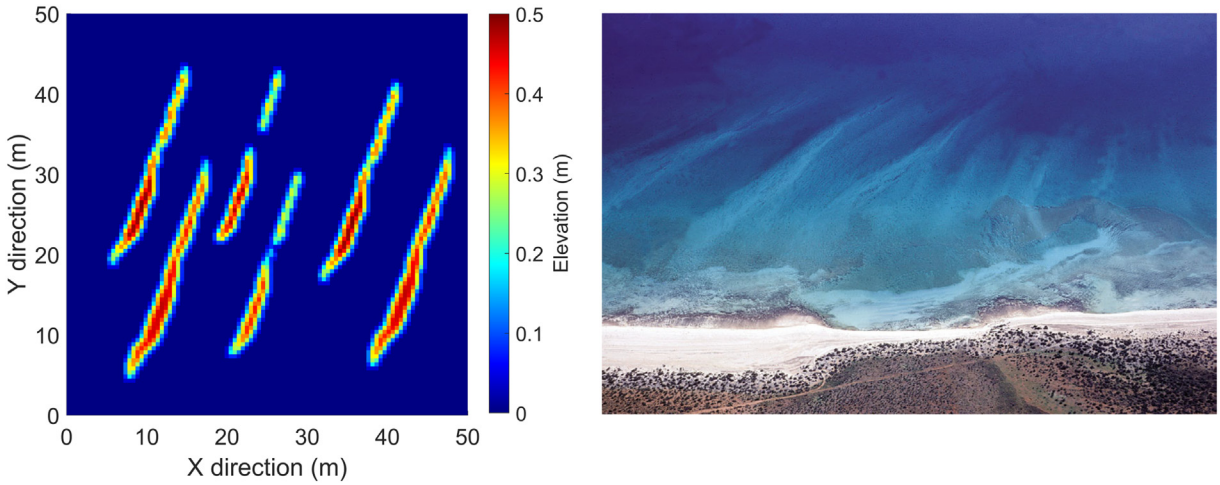

Fig. 16. (left): Input initial surface with elongated ridge-like features. (right): Pleistocene beach ridges with 'fingers' of sand extending into deeper water in Hamelin Pool, Shark Bay, from Playford et al. (2013).

Based on detailed field observations from Highborne Cay in Bahamas, Andres and Reid (2006) recognised two distinct stromatolite morphologies. Columnar stromatolites occur as isolated or coalesced mounds, without a preferred orientation with respect to the shoreline or incoming waves. Stromatolite ridges preferentially occur in shallower back-reef areas, with long axes parallel to the incoming waves. These observations are consistent with results from experiments 1 and 4. Andres and Reid (2006) attribute observed stromatolite occurrence and morphology to differences in rate of accommodation creation, sedimentation patterns, and hydrodynamics. Very similar controls operate in Stromatobyte3D and generate comparable microbialite morphologies within a continuum between columnar forms and ridge-dominated forms. Lateral coalescence is suppressed in the domal end member (experiment 1) due to prominent substrate control that overprinted the hydrodynamic component. As a result, microbialites are gradually buried or smothered by suspended sediment and can't keep up with rising water level. In contrast, when hydrodynamics have strong influence on both growth and sedimentation patterns (experiment 4), in-situ growth is optimised to catch up the water level, and lateral growth is facilitated to trigger lateral mound coalescence to form elongated morphologies. It is the 'dual-control' of accommodation and accretion rate that determine the potential of lateral coalescence, which in turn controls macroscopic mound morphology. In many marine and non-marine microbialites, the frequency of relative water depth changes and duration of subaerial exposure would likely to determine the degree of connections and feedbacks between microbe-dominated ecosystem components, water, and sediment relative to the control by substrate.

If spatial self-organization forms stromatolite ridges in Stromatobyte3D, why do we not see many well-developed ridges or other coherent patterns preserved in ancient strata? Based on these model results, we suspect there are four key reasons. Firstly, ridge formation requires a somewhat complex set of interactions between several processes, so if any of the processes are absent or too weak, or some environmental changes occurred, the fine balance will be changed and ridges will not form. For example, modern stromatolites ridges are found in high-energy water at Promontory Point, Great Salt Lake, separated by channels filled with ooidal sands. In contrast, individual rounded stromatolites are developed on stable substrate in the nearby but more protected Bridger Bay area (Della Porta, 2015; Baskin et al., 2021). Secondly, even if the necessary processes are operating, other processes and factors, currently not considered in this model, may also impact and usually complicate stratigraphic development. For example, erosion is an important process for sculpting microbialites by limiting mound growth, removing accreted microbial deposits, and initiating new phases of microbialite development (Bosak et al., 2013; Paul et al., 2021). Elongated microbialite ridges are interpreted to be a result of wave scour of inter-mound space to prevent mat growth, whereas the adjacent elevated areas are colonised and stabilised by organisms with reduced scour (Logan et al., 1974; Bosak et al., 2013; Playford et al., 2013). Increasing wave scour and abrasion under strong directional flows tends to increase mound relief and produce isolated mounds with regular and smooth edges (Bosak et al., 2013). In contrast, weaker flows and limited scour allow growth to occur in the inter-mound space, causing more irregular mound edges and formation of inter-mound bridge for incipient coalescence. This interpretation is very different from our modelling results, but also important to consider, especially if there is clear evidence of removal of underlying sediment. Faulting, not modelled here, and related sediment disturbance can also be an important factor on microbialite development and distribution on a much larger scale (Andrews and Trewin, 2014; Baskin et al., 2021). Thirdly, the long-term evolution of microbial community can be part of the reason. In fact, agglutinated textures are rare in fossil microbialites, until the relatively recent introduction of diatoms, chlorophytes, and other small algae that significantly increase the mat ability to trap more and coarser sediment, and to resist against erosion (Riding, 2000). Agglutinated microbialites are only well-developed under some specific environmental conditions, which are not easy to achieve (Suarez-Gonzalez et al., 2019), and an even smaller subset of the possible combination of these conditions can generate microbialite ridges. Finally, it may also be that because of the limited nature of exposure, it is often difficult to accurately assess the three-dimensional geometry of stromatolites in some outcrops. Better understanding of how ridge stromatolite structures can form might aid their recognition in outcrop.

As ever, the best approach to any interpretation of ancient strata is likely to be to adopt multiple hypotheses to explain observed morphologies, and then seek further evidence, for example from further outcrop analysis combined with numerical forward modelling, to try to reject or support hypotheses according to this evidence. Following this logic, future work is required to include erosion and other sediment redistributing processes in Stromatobyte3D, and more generally to integrate field-based conceptual models with numerical models to better understand which basic physical, biological, and chemical processes are required to produce specific morphologies, how they interact, and over what spatial and temporal scales.

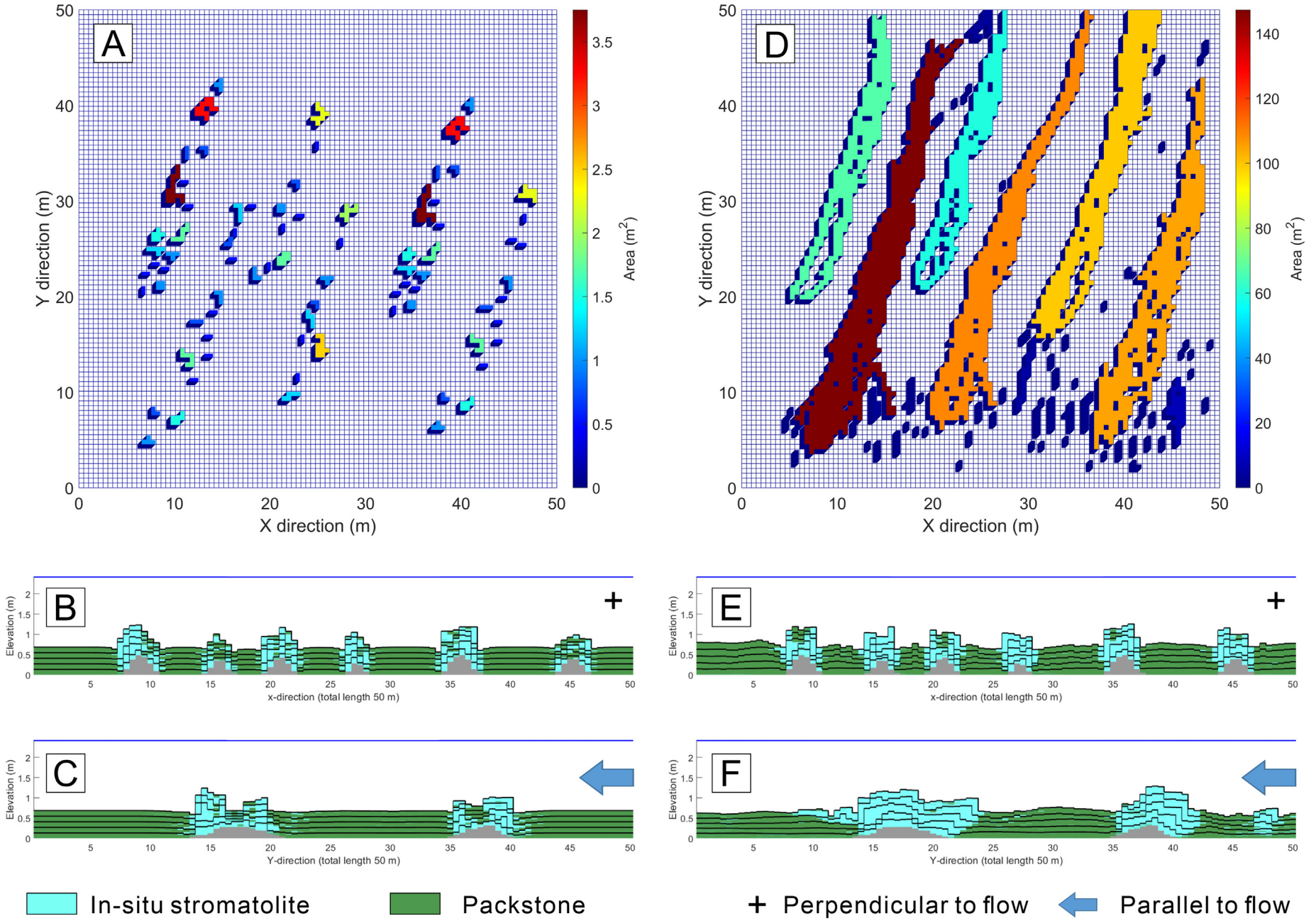

Fig. 17. (A): Map view of experiment 1b after 250 years elapsed model. Microbialite accumulations are colour coded in terms of their 2D connected areas. (B): Cross sections of experiment 1b at Y = 25 m. (C): Cross section of experiment 1b at X = 25 m. (D): Map view of experiment 4b after 250 years elapsed model. (E): Cross sections of experiment 4b at Y = 25 m. (F): Cross section of experiment 4b at X = 25 m. Note how microbialite occurrence is controlled by substrate in both experiments, and how their morphologies change in each experiment due to difference in modelled processes and spatial feedbacks. (For interpretation of the references to colour in this figure legend, the reader is referred to the web version of this article.)

Table 4
Statistics of experiments 1b and 4b, using the same metrics as in experiments 1 to 4.

	Experiment 1b	Experiment 4b
Microbialite vol%	13.1	25.9
Packstone vol%	86.9	74.1
Areal coverage (%)	3.27	26.06
Maximum area (m^2)	4	147
Mean area (m^2)	0.56	0.99
2D connectivity	0.0836	1.5010
Topography correlation coefficient (R)	0.620	0.482

7. Conclusion

Results from this modelling study suggest several significant conclusions:

1. With increasingly strong influence of hydrodynamics on in-situ growth and suspended sediment deposition, three distinct microbialite morphologies are produced in the model, from isolated columns in experiment 1, through longitudinal mounds in experiment 2, to ridges and runnels in experiments 3 and 4, the latter with significantly improved connectivity and anisotropy following the dominant flow direction.
2. Modelled macro-scale microbialite morphologies and distributions are strikingly similar to observations from modern Shark Bay, suggesting modelled processes and their behaviours are realistic, and can therefore be useful explaining how ancient microbialite strata formed.
3. Spatial self-organization can occur in microbialites, similar to coral reefs, in a shallow-water environment affected by shoreline processes with strong wave or current influence, due to interactions between substrate topography, in-situ growth, sedimentation from suspension, and hydrodynamics.
4. Quantitative analysis of mound distribution in map view shows that modelled stromatolite mounds can self-organize to form coherent morphological patterns, independent of initial substrate topography.
5. When the underlying substrate is highly organized with regular morphological features, it may be the dominant control on large scale microbialite occurrence, but self-organizing autogenic dynamics can still impact on individual microbialite growth helping to form and maintain patterns such as elongated morphology parallel to flow direction beyond what would occur simply from the initial substrate control.

Declaration of competing interest

The authors wish to confirm that there are no known conflicts of interest associated with this publication and there has been no significant financial support for this work that could have influenced its outcome.

Acknowledgements

We are grateful to Equinor for providing financial support and permission to publish this work. Dan Bosence and Dave Waltham helped develop the original Mounds3D concepts and model, which are unpublished but very useful for developing this Stromatobyte3D model.

References

Andres, M.S., Reid, R.P., 2006. Growth morphologies of modern marine stromatolites: a case study from Highborne Cay, Bahamas. Sedimentary Geology 185, 319–328.
Andrews, S.D., Trewin, N.H., 2014. Palaeoenvironmental significance of lacustrine stromatolite forms from the Middle Old Red Sandstone of the Orcadian Basin. Geological Magazine 151, 414–429.
Bahniuk, A.M., Anjos, S., Franca, A.B., Matsuda, N., Eiler, J., McKenzie, J.A., Vasconcelos, C., 2015. Development of microbial carbonates in the Lower Cretaceous Codo Formation (north-east Brazil). Implications for interpretation of microbialite facies associations and palaeoenvironmental conditions. Sedimentology 62, 155–181.
Bahniuk, A.M., 2013. Coupling Organic and Inorganic Methods to Study Growth and Diagenesis of Modern Microbial Carbonates, Rio de Janeiro State, Brazil: Implications for Interpreting Ancient Microbialite Facies Development (PhD thesis), ETH, Zurich.
Barabási, A.L., Stanley, H.E., 1995. Fractal Concepts in Surface Growth. Cambridge University Press, Cambridge.
Baskin, R.L., Della Porta, G., Wright, V.P., 2021. Characteristics and controls on the distribution of sublittoral microbial bioherms in Great Salt Lake, Utah: implications for understanding microbialite development. The Depositional Record 1–28.
Beakawi Al-Hashemi, H.M., Baghabra Al-Amoudi, O.S., 2018. A review on the angle of repose of granular materials. Powder Technology 330, 397–417.
Bitzer, K., Salas, R., 2002. SIMSAFADIM; three-dimensional simulation of stratigraphic architecture and facies distribution modeling of carbonate sediments. Computers & Geosciences 28 (10), 1177–1192.
Bosak, T., Knoll, A.H., Petroff, A.P., 2013. The Meaning of Stromatolites. 41 pp. 21–44.
Bouton, A., Vennin, E., Boulle, J., Pace, A., Bourillot, R., Thomazo, C., Brayard, A., Désaubliaux, G., Goslar, T., Yokoyama, Y., Dupraz, C., Visscher, P.T., 2016. Linking the distribution of microbial deposits from the Great Salt Lake (Utah, USA) to tectonic and climatic processes. Biogeosciences 13, 5511–5526.
Burgess, P.M., Wright, V.P., 2003. Numerical forward modeling of carbonate platform dynamics; an evaluation of complexity and completeness in carbonate strata. Journal of Sedimentary Research 73, 637–652.
Burne, R.V., Moore, L.S., 1987. Microbialites; organosedimentary deposits of benthic microbial communities. PALAIOS 2, 241–254.
Carvalho, C., Oliveira, M.I.N., Macario, K., Guimarães, R.B., Keim, C.N., Sabadini-Santos, E., Crapez, M.A.C., 2018. Stromatolite growth in Lagoa Vermelha, southeastern coast of Brazil: evidence of environmental changes. Radiocarbon 60, 383–393.
Coshell, L., Rosen, M.R., Mcnamara, K.J., 1998. Hydromagnesite Replacement of Biomineralized Aragonite in a New Location of Holocene Stromatolites, Lake Walyungup, Western Australia. 45 pp. 1005–1018.
Coulson, K.P., 2016. Microbialite elongation by means of coalescence: an example from the middle Furongian (upper Cambrian) Notch Peak Formation of western Utah. Facies 62, 20.
Curtis, A., Wood, R., Bowyer, F., Shore, A., Curtis-Walcott, A., Robertsson, J., 2021. Modelling Ediacaran metazoan–microbial reef growth. Sedimentology 68, 1877–1892.
Della Porta, G., 2015. Carbonate build-ups in lacustrine, hydrothermal and fluvial settings: comparing depositional geometry, fabric types and geochemical signature. In: Bosence, D.W.J., Gibbons, K.A., Heron, D.P.L., Morgan, W.A., Pritchard, T., Vining, B.A. (Eds.), Microbial Carbonates in Space and Time: Implications for Global Exploration and Production. vol. 418. Geological Society of London, p. 0.
Dill, R.F., Shinn, E.A., Jones, A.T., Kelly, K., Steinen, R.P., 1986. Giant subtidal stromatolites forming in normal salinity waters. Nature 324, 55–58.
Dravis, J.J., 1983. Hardened subtidal stromatolites, Bahamas. Science 219, 385–386.
Dupraz, C., Reid, R.P., Braissant, O., Decho, A.W., Norman, R.S., Visscher, P.T., 2009. Processes of carbonate precipitation in modern microbial mats. Earth-Science Reviews 96, 141–162.
Gallois, A., Bosence, D., Burgess, P.M., 2018. Brackish to hypersaline facies in lacustrine carbonates: Purbeck Limestone Group, Upper Jurassic–Lower Cretaceous, Wessex Basin, Dorset, UK. Facies 64, 12.
Gebelein, C.D., 1969. Distribution, morphology, and accretion rate of recent subtidal algal stromatolites, Bermuda. Journal of Sedimentary Research 39, 49–69.
Ginsburg, R.N., Planavsky, N.J., 2008. Diversity of Bahamian microbialite substrates. In: Dilek, Y., Furnes, H., Muehlenbachs, K. (Eds.), Links Between Geological Processes, Microbial Activities & Evolution of Life: Microbes and Geology. Springer Netherlands, Dordrecht, pp. 177–195.
Grotzinger, J.P., Knoll, A., 1999. Stromatolites in Precambrian carbonates: evolutionary mileposts or environmental dipsticks? The Annual Review of Earth and Planetary Sciences 27, 313–358.
Grotzinger, J.P., Rothman, D.H., 1996. An abiotic model for stromatolite morphogenesis. Nature 383, 423–425.
Hoffman, P., 1974. Shallow and deepwater stromatolites in Lower Proterozoic platform–to–basin facies change, Great Slave Lake, Canada. AAPG Bulletin 58, 856–867.
Jahnert, R.J., Collins, L.B., 2012. Characteristics, distribution and morphogenesis of subtidal microbial systems in Shark Bay, Australia. Marine Geology 303-306, 115–136.
Johnson, J., Grotzinger, J.P., 2006. Affect of sedimentation on stromatolite reef growth and morphology, Ediacaran Omkyk Member (Nama Group), Namibia. South African Journal of Geology 109, 87–96.
Kozlowski, E., 2016. Multi-scale Forward Modelling of Microbial Lacustrine Carbonates. Royal Holloway, University of London (PhD thesis).
Leach, R., 2014. Chapter 8 - surface topography characterisation. Fundamental Principles of Engineering Nanometrology, Second edition, pp. 241–294.
Levin, S.A., Segel, L.A., 1985. Pattern Generation in Space and Aspect. 27 pp. 45–67.
Logan, B.W., 1961. Cryptozoon and Associate Stromatolites from the Recent, Shark Bay, Western Australia. The Journal of Geology 69, 517–533.
Logan, B.W., Hoffman, P., Gebelein, C.D., 1974. Algal mats, cryptalgal fabrics, and structures, Hamelin Pool, Western Australia. Evolution and Diagenesis of Quaternary Carbonate Sequences, Shark Bay, Western Australia, pp. 140–194.
Martinez, P.A., Harbaugh, J.W., 1989. Computer simulation of wave and fluvial-dominated nearshore environments. In: Lakhan, V.C., Trenhaile, A.S. (Eds.), Elsevier Oceanography Series. vol. 49. Elsevier, pp. 297–340.
Monty, C.L.V., 1976. Chapter 5.1 the origin and development of cryptalgal fabrics. In: Walter, M.R. (Ed.), Developments in Sedimentology. vol. 20. Elsevier, pp. 193–249.
Parellada, A.L., 2016. Holocene Evolution of the Microbial Deposits in the Clifton-Preston Lake System, Western Australia (Master thesis), Curtin University.
Paul, A., Lokier, S.W., Sherry, A., Andrade, L.L., Court, W.M., van der Land, C., Dutton, K.E., Head, I.M., 2021. Erosion-initiated Stromatolite and Thrombolite Formation in a Present-day Coastal Sabkha Setting. 68 pp. 382–401.

Paull, C.K., Neumann, A.C., Bebout, B., Zabielski, V., Showers, W., 1992. Growth rate and stable isotopic character of modern stromatolites from San Salvador, Bahamas. Palaeogeography, Palaeoclimatology, Palaeoecology 95, 335–344.
Playford, P.E., Cockbain, A.E., Berry, P.F., Roberts, A.P., Haines, P.W., Brooke, B.P., 2013. The Geology of Shark Bay. Geological Survey of Western Australia: Bulletinvol. 146.
Purdy, E.G., Bertram, G.T., 1993. Carbonate Concepts From the Maldives, Indian Ocean. American Association of Petroleum Geologists.
Purkis, S.J., Casini, G., Hunt, D., Colpaert, A., 2015. Morphometric patterns in Modern carbonate platforms can be applied to the ancient rock record: similarities between Modern Alacranes Reef and Upper Palaeozoic platforms of the Barents Sea. Sedimentary Geology 321, 49–69.
Purkis, S.J., Koppel, J.V.D., Burgess, P.M., 2016. Spatial self-organization in carbonate depositional environments. In: Budd, D.A., Hajek, E.A., Purkis, S.J. (Eds.), Autogenic Dynamics and Self-organization in Sedimentary Systems. SEPM Society for Sedimentary Geologyvol. 106.
Reid, R.P., Visscher, P.T., Decho, A.W., Stolz, J.F., Bebout, B.M., Dupraz, C., Macintyre, I.G., Paerl, H.W., Pinckney, J.L., Prufert-Bebout, L., Steppe, T.F., DesMarais, D.J., 2000. The role of microbes in accretion, lamination and early lithification of modern marine stromatolites. Nature 406, 989–992.
Reitner, J., 2011. Microbial mats. In: Reitner, J., Thiel, V. (Eds.), Encyclopedia of Geobiology. Springer Netherlands, Dordrecht, pp. 606–608.
Riding, R., 2000. Microbial carbonates: the geological record of calcified bacterial–algal mats and biofilms. Sedimentology 47, 179–214.
Riding, R., 2011a. The nature of stromatolites: 3,500 million years of history and a century of research. In: Reitner, J., Quéric, N.-V., Arp, G. (Eds.), Advances in Stromatolite Geobiology. Springer Berlin Heidelberg, Berlin, Heidelberg, pp. 29–74.
Riding, R., 2011b. Microbialites, stromatolites, and thrombolites. In: Reitner, J., Thiel, V. (Eds.), Encyclopedia of Geobiology. Springer Netherlands, Dordrecht, pp. 635–654.
Rietkerk, M., van de Koppel, J., 2008. Regular pattern formation in real ecosystems. Trends in Ecology & Evolution 23, 169–175.
Sadler, P.M., 1981. Sediment Accumulation Rates and the Completeness of Stratigraphic Sections. 89 pp. 569–584.
Schlager, W., 1999. Scaling of sedimentation rates and drowning of reefs and carbonate platforms. Geology 27, 183–186.
Schlager, W., Purkis, S., 2013. Bucket structure in carbonate accumulations of the Maldive, Chagos and Laccadive archipelagos. International Journal of Earth Sciences 102, 2225–2238.
Schlager, W., Purkis, S., 2015. Reticulate reef patterns – antecedent karst versus self-organization. Sedimentology 62, 501–515.
Suarez-Gonzalez, P., Benito, M.I., Quijada, I.E., Mas, R., Campos-Soto, S., 2019. 'Trapping and binding': a review of the factors controlling the development of fossil agglutinated microbialites and their distribution in space and time. Earth-Science Reviews 194, 182–215.
Suosaari, E.P., Reid, R.P., Playford, P.E., Foster, J.S., Stolz, J.F., Casaburi, G., Hagan, P.D., Chirayath, V., Macintyre, I.G., Planavsky, N.J., Eberli, G.P., 2016. New multi-scale perspectives on the stromatolites of Shark Bay, Western Australia. Scientific Reports 6, 20557.
Turing, A.M., 1952. The chemical basis of morphogenesis. Philosophical Transactions of the Royal Society of London B 237, 37–72.
van de Vijsel, R.C., van Belzen, J., Bouma, T.J., van der Wal, D., Cusseddu, V., Purkis, S.J., Rietkerk, M., van de Koppel, J., 2019. Estuarine Biofilm Patterns: Modern Analogues for Precambrian Self-organization. 45 pp. 1141–1154.
Warren, J.K., 1982. The hydrological significance of Holocene tepees, stromatolites, and boxwork limestones in coastal salinas in South Australia. Journal of Sedimentary Research 52, 1171–1201.
Wood, R.A., Grotzinger, J.P., Dickson, J.A.D., 2002. Proterozoic Modular Biomineralized Metazoan From the Nama Group, Namibia. 296 pp. 2383–2386.
Xi, H., Burgess, P.M., 2022. The stratigraphic significance of self-organization: exploring how autogenic processes can generate cyclical carbonate platform strata. Sedimentology https://doi.org/10.1111/sed.12974 In press.